can thus explain the magic numbers of the mass spectrum, but not the size-dependence of T_{melt} and q.

For large sodium clusters of several thousand atoms, geometrical shell closings can explain the intensities in a mass spectrum[9]. But smaller clusters could also have an icosahedral structure, and although this does not show up in the mass spectrum, it might well have an influence on the cluster melting points. There is an icosahedral shell closing at 147 atoms, and indeed the latent heat has a pronounced maximum in this region. However, it is not possible to explain all the observed features by geometrical models, either by the icosahedral structure mentioned above, or by the modified pentagonal bipyramid structures favoured by gold clusters in this size range[15]. Thus geometrical shell closing arguments cannot explain the size dependence of either T_{melt} or q.

We therefore conclude that the size dependence of melting-point temperature and latent heat of fusion cannot be explained by one simple argument. There is probably a complicated interplay between geometric and electronic structure, presenting a challenge for theory. □

Received 8 December 1997; accepted 16 February 1998.

1. Pawlow, P. Über die Abhängigkeit des Schmelzpunktes von der Oberflächenenergie eines festen Körpers. *Z. Phys. Chem.* **65,** 1–35 (1909).
2. Couchman, R. R. The Lindemann hypothesis and the size dependence of melting temperatures II. *Phil. Mag. A* **40,** 637–643 (1979).
3. Berry, R. S. When the melting and freezing point are not the same. *Sci. Am.* **263,** 50–56 August (1990).
4. Buffat, Ph. & Borel, J. P. Size effect on the melting temperature of gold clusters. *Phys. Rev. A* **13,** 2287–2298 (1976).
5. Lai, S. L., Guo, J. Y., Petrova, V., Ramanath, G. & Allen, L. H. Size-dependent melting properties of small tin particles: nonocalorimetric measurements. *Phys. Rev. Lett.* **77,** 99–102 (1996).
6. Schmidt, M., Kusche, R., Kronmüller, W., v. Issendorff, B. & Haberland, H. Experimental determination of the melting point and heat capacity for a free cluster of 139 sodium atoms. *Phys. Rev. Lett.* **79,** 99–102 (1997).
7. Bertsch, G. Melting in clusters. *Science* **277,** 1619 (1997).
8. Hovick, J. W. & Bartell, L. S. Phase and phase-changes in tert-butyl thiol. *J. Mol. Struct.* **413,** 615–620 (1997).
9. Martin, T. P. Shells of atoms. *Phys. Rep.* **273,** 199–241 (1996).
10. Buck, U. & Ettischer, I. Experimental evidence for an isomeric transition of size selected methanol hexamers. *J. Chem. Phys.* **100,** 6974–6976 (1994).
11. Ellert, Ch., Schmidt, M., Schmitt, Ch., Reiners, Th. & Haberland, H. Temperature dependence of the optical response of small, open shell sodium clusters. *Phys. Rev. Lett.* **75,** 1731–1734 (1995).
12. Wales, D. J. & Berry, R. S. Freezing, melting, spinodals, and clusters. *J. Chem. Phys.* **92,** 4473–4481 (1990).
13. de Heer, W. A. The physics of simple metal clusters: experimental aspects and simple models. *Rev. Mod. Phys.* **65,** 611–676 (1993).
14. Brack, M. The physics of simple metal clusters: self-consistent jellium model and semi-classical approaches. *Rev. Mod. Phys.* **65,** 677–732 (1993).
15. Cleveland, C. L. *et al.* Structural evolution of smaller gold nanocrystals: the truncated decahedral motif. *Phys. Rev. Lett.* **79,** 1873–1876 (1997).

Acknowledgements. This work was supported by the Deutsche Forschungsgemeinschaft.

Correspondence and requests for materials should be addressed to H.H. (e-mail: hellmut@frha06.physik.uni-freiburg.de).

Carbon nanotubes as long ballistic conductors

C. T. White*† & T. N. Todorov*

** Department of Materials, University of Oxford, Parks Road, Oxford OX1 3PH, UK*

Early theoretical work on single-walled carbon nanotubes[1–3] predicted that a special achiral subset of these structures known as armchair nanotubes[3] should be metallic. Tans *et al.*[4] have recently confirmed these predictions experimentally and also showed directly that coherent electron transport can be maintained through these nanowires up to distances of at least 140 nm. But single-walled armchair nanotubes are one-dimensional conductors with only two open conduction channels (energy subbands in a laterally confined system that cross the Fermi level)[1–3]. Hence, with increasing length, their conduction electrons ultimately become localized[5] owing to residual disorder in the tube which is inevitably produced by interactions between the tube and its environment. We present here calculations which show, however, that unlike normal metallic wires, conduction electrons in armchair nanotubes experience an effective disorder averaged over the tube's circumference, leading to electron mean free paths that increase with nanotube diameter. This increase should result in exceptional ballistic transport properties and localization lengths of 10 μm or more for tubes with the diameters that are typically produced experimentally[6].

Once physisorbed on a surface, even an initially perfect metallic carbon nanotube is disordered because of residual interactions with the substrate. In general, for such long thin conductors at zero temperature, the theory of transport through weakly disordered materials predicts a transition to a localized regime (where the resistance R is exponentially large) around a wire length where R reaches a value of one quantum resistance unit[7], $r = h/2e^2$. Deep within the localized regime the resistance increases exponentially with length L as $R(L) \sim e^{L/\xi}$, where ξ is the localization length for electrons in the disordered wire[8]. For wires with N_C open conduction channels, ξ is given within a factor of order unity by $\xi = N_C l$ (refs 9, 10) where l is the elastic mean free path for backward electron scattering. Hence for wires with $N_C \gg 1$, the motion of the electron on the scale of ξ is largely diffusive, but for weakly disordered, small-diameter armchair nanotubes, which have $N_C = 2$, this motion is largely ballistic. This analysis suggests immediately that any observable quantum transport through these nanotubes is also ballistic.

For a fixed amount of disorder, as the transverse size of a normal metallic quantum wire increases l remains largely fixed but ξ increases due to the introduction of new channels at the Fermi level, ϵ_F (see ref. 10 and refs therein). However, this behaviour does not lead to long localization lengths in armchair carbon nanotubes because N_C remains pinned at two. We will show, however, that for a fixed amount of disorder as the radius of a small-diameter armchair tube increases, l does not remain fixed but rather increases leading to long localization lengths. We will also show that this remarkable behaviour arises because of the special character of the armchair states close to ϵ_F in the perfect tube and hence does not depend crucially on the details of the disorder.

To study the effects of disorder on the transport properties of armchair nanotubes we adopt the usual tight-binding model which retains only the nearest neighbour π-like hamiltonian matrix elements between $|p_\perp\rangle$ orbitals (one per carbon atom) orientated normal to the tubule surface[1,3]. Local density-functional calculations have established that this model, with all diagonal matrix elements fixed at ϵ_F and all non-zero off-diagonal matrix elements fixed at $V_0 = -2.7$ eV provides an excellent description of the valence bands of perfect armchair carbon nanotubes in the vicinity of ϵ_F (refs 1, 11). The effects of disorder can then be incorporated into the model (referred to here as the 'full model') by assuming that these diagonal and off-diagonal matrix elements are not fixed at their values in the perfect tube but are independent random variables with variances σ_ϵ^2 and σ_V^2, respectively.

In the absence of disorder, the full model yields $2N_B$ bands as a function of the quasi-momentum k that labels an eigenstate of the helical screw operator $S(\theta_0, z_0)$ used to generate the $[N_B, N_B]$ armchair tube by starting with a single ring, such as highlighted in Fig. 1a, and then rotating this ring by $\theta_0 = \pi/N_B$ radians around the tubule axis followed by a translation $z_0 = (\sqrt{3}/2)d_0$ along this axis[11]. Each ring contains $2N_B$ carbon atoms and has a radius $r_T = (3d_0/2\pi)N_B$, where N_B is the number of C–C bonds in the ring and $d_0 = 0.142$ nm is the C–C bond distance. The a_1 and a_2 bands that cross at $k_F = 2\pi/3$ are present in all armchair tubules[1]. These two bands are highlighted in Fig. 1b for the [10,10] tube. In the absence of disorder, symmetry can be used to block diagonalize the full model to the point that the a_1 and a_2 bands are described

† Permanent address: Code 6179, Naval Research Laboratory, Washington DC 20375, USA.

exactly (within an unimportant constant) by the hamiltonian:

$$H_0 = V_0 \sum_{j=1}^{2} (-1)^{(j+1)} \left[\sum_m [|a_{jm}\rangle\langle a_{jm}| + (|a_{jm}\rangle\langle a_{j(m+1)}| + \text{H.c.})] \right] \quad (1)$$

where $|a_{1m}\rangle$ ($|a_{2m}\rangle$) denotes the a_1 (a_2) state constructed from rotationally invariant—under C_{N_B} rotations—symmetric (antisymmetric) sums of $|p_\perp\rangle$ orbitals for each of the N_B pairs of nearest neighbours in the $2N_B$ atom carbon ring labelled m and H.c. is the Hermitian conjugate.

Breaking the symmetries used to derive equation (1), disorder introduces additional couplings not only between the states making up the a_1 and a_2 bands but also between these states and states making up the other $2(N_B - 1)$ bands present in the full model. However, for small-diameter tubes these other bands are separated by at least $\pm\pi V_0/N_B$ from ϵ_F. Hence, if the disorder is not too severe and r_T not too large, we should still be able to work entirely within the reduced basis that describes the a_1 and a_2 bands. With this approximation we arrive at a two-band model for studying the transport properties of small-diameter, weakly disordered armchair nanotubes at and around ϵ_F. The hamiltonian describing this reduced model is given by $H = H_0 + U$, where U is the projection onto the reduced two-band basis of the perturbation introduced by the disorder into the full model.

In its most general form H is given by:

$$H = \sum_m \left\{ \sum_{j=1}^{2} \left\{ (\bar{\epsilon}_m + (-1)^{(j+1)} \widehat{V}_m) |a_{jm}\rangle\langle a_{jm}| + [(-1)^{(j+1)} \overline{V}_m |a_{jm}\rangle\langle a_{j(m+1)}| + \text{H.c.}] \right\} + [\bar{\epsilon} |a_{1m}\rangle\langle a_{2m}| + \widetilde{V}_m (|a_{1m}\rangle\langle a_{2(m+1)}| - |a_{2m}\rangle\langle a_{1(m+1)}|) + H.c.] \right\} \quad (2)$$

where $\bar{\epsilon}_m = (1/N_B)\Sigma_{n=1}^{N_B}(V^{11}_{mnmn} + V^{22}_{mnmn})/2$; $\tilde{\epsilon}_m = (1/N_B)\Sigma_{n=1}^{N_B} \times (V^{11}_{mnmn} - V^{22}_{mnmn})/2$; $\hat{V}_m = (1/N_B)\Sigma_{n=1}^{N_B} V^{12}_{mnmn}$; $\bar{V}_m = (1/N_B)\Sigma_{n=1}^{N_B} \times (V^{21}_{mn(m+1)n} + V^{12}_{mn(m+1)(n-1)})/2$; $\tilde{V}_m = (1/N_B)\Sigma_{n=1}^{N_B}(V^{21}_{mn(m+1)n} - V^{12}_{mn(m+1)(n-1)})/2$, and the prefactors of $1/N_B$ arise from the normalization of the ring states. The matrix elements V^{ij}_{pqmn} are defined by $V^{ij}_{pqmn} = \langle pq; i|H_T|mn; j\rangle$, where $|mn;1\rangle$ ($|mn;2\rangle$) denotes the $|p_\perp\rangle$ orbital associated with the carbon labelled 1 (2) in the C–C bond labelled n modulo N_B in the ring labelled m. In this notation the C–C bond defined by n and m' is located by rotating and translating the two carbon atoms in the C–C bond defined by n and m by $(m' - m)$ applications of $S(\theta_0, z_0)$. Finally, H_T denotes the full model hamiltonian in the presence of disorder. Hence the disorder introduced into H_T manifests itself in H as averages of the matrix elements of H_T over the number of carbon bonds in a ring.

For the two-band model in the weak scattering limit l is given with the aid of Fermi's golden rule by:

$$\frac{1}{l} = \frac{2\pi}{v_F \hbar} \left[\frac{1}{2} \sum_{j,j'=1}^{2} \left\langle \left| \langle k_{jF}|[H - \langle H\rangle]|(-1)^{(j-j'+1)} k_{j'F}\rangle \right|^2 \right\rangle \right] \rho(\epsilon_F), \quad (3)$$

where l is measured in number of rings along the tube, $v_F = \sqrt{3}|V_0|/\hbar$, $\langle \cdots \rangle$ denotes an ensemble average over the disordered potentials, $|k_{jF}\rangle = (1/\sqrt{N})\Sigma_m e^{imk_F}|a_{jm}\rangle$ with $k_F = 2\pi/3$, H is defined by equation (2), and $\rho(\epsilon_F) = N/2\pi\sqrt{3}|V_0|$ is the density of back scattered states at ϵ_F for either the a_1 or a_2 bands for a tube containing N rings in the limit of large N. Equation (3) yields:

$$l = \frac{6V_0^2}{(2\sigma_\epsilon^2 + 9\sigma_V^2)} N_B. \quad (4)$$

In arriving at equation (4) we have repeatedly used the relation $\langle (1/N_B^2)\Sigma_{i,j=1}^{N_B}[(x_i - x_0)(x_j - x_0)]\rangle = \sigma_x^2/N_B$ valid for independent random variables x_i with average x_0 and variance σ_x^2. The derivation of equation (4) requires that the two-band model is valid and hence that the disordered diagonal and off-diagonal matrix elements of H have standard deviations ($\sigma_\epsilon/\sqrt{N_B}$, $\sigma_V/\sqrt{N_B}$) that are small with respect to $\pi|V_0|/N_B = \sqrt{3}|V_0|d_0/2r_T$ or equivalently $\max(\sigma_\epsilon, \sigma_V) \ll \sqrt{3}\pi d_0/2r_T|V_0|$. Hence, if the disorder—measured by $\max(\sigma_\epsilon, \sigma_V)$—is not too severe and r_T not too large, equation (4) should be valid. But for small-diameter residually disordered tubes this constraint, which prevents the a_1 and a_2 states at ϵ_F from mixing appreciably with the other bands of the full model, should be satisfied. In particular, for the [10,10] tube it becomes, $\max(\sigma_\epsilon, \sigma_V) \ll \pi|V_0|/\sqrt{10} = 2.7$ eV.

Equation (4) predicts that weakly disordered small-diameter armchair tubules differ fundamentally from normal metallic wires which have electron mean free paths along the wire independent of the wire's transverse size. In a normal metallic wire the disorder-induced variance of the hamiltonian matrix elements between transverse wire states will contain a factor analogous to N_B^{-1} for the tube. However, in such a wire the number of open conduction channels, N_C, at ϵ_F will grow as N_B and hence so too will the total density of states, making l independent of the wire's transverse size. In contrast, for armchair nanotubes, N_C is fixed at two, the density

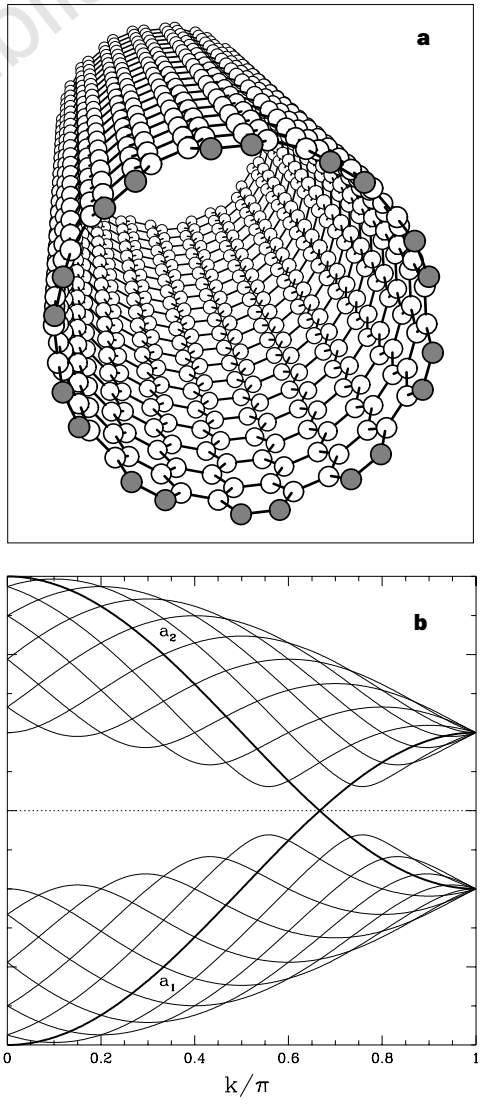

Figure 1 Geometry and band structure of the [10,10] armchair nanotube. **a**, A segment of the [10,10] armchair tubule with a planar 20-atom carbon ring containing 10 C–C bonds that can be used to generate the entire tubule depicted in grey. **b**, Band structure of the perfect [10,10] tubule within the full model. The a_1 and a_2 bands which cross at ϵ_F (≡0.0 eV) are depicted as heavy lines.

of states does not contain the compensating factor for N_B^{-1}, and l will grow as N_B. Equation (4) also predicts the small-diameter, weakly disordered armchair nanotubes—with N_C pinned at 2—will have localization lengths (given by $\xi \approx N_C l$) that are comparable to those in similarly disordered normal wires with similar Fermi velocities but with $N_C = 2N_B$. Finally, equation (4) predicts that residually disordered tubes will show ballistic electron transport over unprecedented distances for such laterally confined systems. This follows because the chemical and mechanical stability of the tube make σ_ϵ^2 and σ_V^2 small, the strong C–C interaction makes $|V_0|$ large, and the special character of the armchair states at ϵ_F enhances l by a factor of N_B.

As an example of the last prediction, we consider a positionally disordered tube ($\sigma_\epsilon = 0$ eV, $\sigma_V \neq 0$ eV) where the C–C bond lengths vary according to a rectangular probability distribution by as much as ±1% of d_0. Because the off-diagonal matrix elements of the full model should change with C–C bond length as in polyacetylene[1] ($\delta V = \alpha \delta d$ with $\alpha \approx 47\,\mathrm{eV\,nm^{-1}}$), σ_V will be ~0.04 eV. Equation (4) then yields $l = 3.7\,\mu$m ($\xi \approx 7.5\,\mu$m) for $V_0 = -2.7$ eV and $N_B = 10$. As an additional example, we consider a substitutionally disordered tube ($\sigma_\epsilon \neq 0$ eV, $\sigma_V = 0$ eV) where the probability of finding an impurity with potential ϵ_a is given by P. If the impurities correspond to nitrogen atoms ($\epsilon_a = -2.5$ eV; ref. 12) separated on average by 10 nm along the [10,10] tube ($P = 6.0 \times 10^{-4}$), then $\sigma_\epsilon = \sqrt{P(1-P)}|\epsilon_a| = 0.06$ eV and equation (4) yields $l = 7.5\,\mu$m ($\xi \approx 15\,\mu$m) for $V_0 = -2.7$ eV and $N_B = 10$.

Substrate interactions are not expected to significantly flatten tubes such as the [10,10] (ref. 13). In addition, twists along the tube are unlikely to be produced by its van der Waals interaction with the substrate. On the other hand, bends caused by nanometre- (or larger-) scale substrate features can occur and could limit l (ref. 4). The principal effect of a bend will be to shift the inter-ring matrix elements contributing to $\overline{V}_m$ and V_m in equation (2). However, for every such matrix element in the full model that is increased by a small amount by the bend there is a corresponding one decreased by approximately the same amount, leaving $\bar{V}_m$ and $\tilde{V}_m$ largely unchanged. Thus, bends result in little if any scattering of the conduction electrons[14] and small-diameter armchair nanotubes should behave as true electron waveguides.

The unconventional scaling rule proposed here predicts exceptional ballistic transport properties for single-walled weakly disordered armchair nanotubes. This prediction can be understood in physical terms as follows. In the weak scattering limit, electrons injected at ϵ_F enter ring states making up the a_1 and a_2 bands that are rotationally invariant under C_{N_B} rotations about the $[N_B,N_B]$ tubule axis. For small-diameter tubes, scattering of these conduction electrons by the disorder is only between ring states of this symmetry due to energy conservation. However, any linear combination of these ring states extends around the full circumference of the tube. Thus, the closest we can come to a classical picture of a nanotube conduction electron in the two-band basis is a doughnut-like wave packet confined along the tube but extended around its circumference. This 'doughnut' wave packet experiences an effective disorder that is an average of the real disorder over the tube's circumference ($\propto N_B$). The mean square amplitude of this effective disorder is then reduced relative to that of the real disorder by a factor of N_B whenever the real disorder fluctuates on the scale of a carbon–carbon bond length. Hence—so long as the two-band model remains valid—the larger the tube's diameter grows, the greater the reduction and the more freely the 'doughnut' wave packet propagates along the tube leading to an enhancement of l by a factor of N_B. For [10,10] nanotubes which have $N_B = 10$, this enhancement is large, affording the opportunity for directly observing ballistic electron transport over unprecedented distances for such laterally confined systems[4]. We do not expect that electron–electron interactions will alter this conclusion because spin-split states should still average the disorder over the circumference of the tube. □

Received 30 October 1997; accepted 23 February 1998.

1. Mintmire, J. W., Dunlap, B. I. & White, C. T. Are fullerene tubules metallic? *Phys. Rev. Lett.* **68,** 631–634 (1992).
2. Hamada, N., Sawada, A. & Oshiyama, A. New one-dimensional conductors: graphitic micro-tubules. *Phys. Rev. Lett.* **68,** 1579–1581 (1992).
3. Saito, R., Fujita, M., Dresselhaus, G. & Dresselhaus, M. S. Electronic structure of chiral graphene tubules. *Appl. Phys. Lett.* **60,** 2204–2206 (1992).
4. Tans, S. J. *et al.* Individual single-wall carbon nanotubes as quantum wires. *Nature* **386,** 474–477 (1997).
5. Mott, N. F. & Twose, W. D. The theory of impurity conduction. *Adv. Phys.* **10,** 107–163 (1961).
6. Tess, A. *et al.* Crystalline ropes of metallic carbon nanotubes. *Science* **273,** 483–487 (1996).
7. Thouless, D. J. Maximum metallic resistance in this wires. *Phys. Rev. Lett.* **39,** 1167–1169 (1977).
8. Anderson, P. W., Thouless, D. J., Abrahams, E. & Fisher, D. S. New method for a scaling theory of localization. *Phys. Rev. B* **22,** 3519–3526 (1980).
9. Thouless, D. J. Localization distance and mean free path in one-dimensional disordered systems. *J. Phys. C* **6,** L46–L51 (1973).
10. Todorov, T. N. Calculation of the residual resistivity of three-dimensional quantum wires. *Phys. Rev. B* **54,** 5801–5813 (1996).
11. White, C. T., Robertson, D. H. & Mintmire, J. W. Helical and rotational symmetries of nanoscale graphitic tubules. *Phys. Rev. B* **47,** 5485–5488 (1993).
12. Harrison, W. A. *Electronic Structure and Properties of Solids* 550 (Freeman, San Francisco, 1980).
13. Ruoff, R. S. *et al.* Radial deformation of carbon nanotubes by van der Waals forces. *Nature* **364,** 514–516 (1993).
14. Kane, C. L. & Mele, E. J. Size, shape, and low energy electronic structure of carbon nanotubes. *Phys. Rev. Lett.* **78,** 1932–1935 (1997).

Acknowledgements. C.T.W. thanks D. G. Pettifor for hospitality during his sabbatical stay at Oxford and N. J. Long and D. H. Robertson for technical assistance. T.N.T. thanks EPSRC and St John's College, Oxford for support. Support from the US Office of Naval Research and Hewlett Packard is also acknowledged.

Correspondence and requests for materials should be addressed to C.T.W. at NRL (e-mail: white@alchemy.nrl.navy.mil).

Intertwined symmetry of the magnetic modulation and the flux-line lattice in the superconducting state of $TmNi_2B_2C$

M. R. Eskildsen*, K. Harada†, P. L. Gammel‡, A. B. Abrahamsen*, N. H. Andersen*, G. Ernst‡, A. P. Ramirez‡, D. J. Bishop‡, K. Mortensen*, D. G. Naugle§, K. D. D. Rathnayaka§ & P. C. Canfield‖

* *Risø National Laboratory, PO Box 49, DK-4000 Roskilde, Denmark*
† *Advanced Research Laboratory, Hitatchi Ltd, Hatoyama, Saitama 350-03, Japan*
‡ *Bell Laboratories, Lucent Technologies, 700 Mountain Avenue, Murray Hill, New Jersey 07974, USA*
§ *Physics Department, Texas A&M University, College Station, Texas 77843, USA*
‖ *Ames Laboratory and Department of Physics and Astronomy, Iowa State University, Ames, Iowa 50011, USA*

Materials that can in principle exhibit both superconductivity and ferromagnetism are caught in a dilemma: both states represent long-range order, but are in general mutually exclusive. When the material favours a ground state with a large magnetic moment, as is the case for Er_4Rh_4B (ref. 1), superconductivity is destroyed. For superconductivity to persist, the magnetic structure would need to adopt an antiferromagnetic modulation of short enough wavelength to ensure a small net moment on the length scale of the superconducting coherence length. The intermetallic borocarbide superconductors[2–4] RNi_2B_2C (where R is a rare-earth element) have shed new light on this balance between magnetism and superconductivity. The response of these materials in the superconducting state to a magnetic field is dominated by the formation of a flux-line lattice—a regular array of quantized magnetic vortices whose symmetry and degree of order are easily modified and thus can be expected to interact with an underlying